CAPÍTULO 9

doi

MCNPX DOSIMETRY AND RADIATION-INDUCED CANCER RISK ESTIMATION FROM ^{18}F-FDG PEDIATRIC PET IN THE BRAZILIAN POPULATION

Data de aceite: 01/07/2020

Data de submissão: 12/06/2020

Bruno Melo Mendes
Centro de Desenvolvimento da Tecnologia Nuclear, CDTN.
Belo Horizonte, MG.
http://lattes.cnpq.br/7016638154017973

Andréa Vidal Ferreira
Centro de Desenvolvimento da Tecnologia Nuclear, CDTN.
Belo Horizonte, MG.
http://lattes.cnpq.br/8661579024063656

Telma Cristina Ferreira Fonseca
Universidade Federal de Minas Gerais – UFMG.
Belo Horizonte, MG.
http://lattes.cnpq.br/3139727297057976

Bruno Machado Trindade
Universidade Federal de Minas Gerais – UFMG.
Belo Horizonte, MG.
http://lattes.cnpq.br/6883132705715860

Tarcísio Passos Ribeiro de Campos
Universidade Federal de Minas Gerais – UFMG.
Belo Horizonte, MG.
http://lattes.cnpq.br/2004647037137301

ABSTRACT: Positron emission tomography (PET) using ^{18}F-FDG has increased significantly in pediatric patients. PET with ^{18}F-FDG has often been applied in oncology. Cancer induction is one of the main stochastic risks from exposure to ionizing radiation of ^{18}F-FDG. Radiation-induced cancer risk estimation due to medical exposures is an important tool for risk/benefit assessing. The objective was to perform dosimetry and estimate the risk of cancer induction due to pediatric use of ^{18}F-FDG. MCNPx Computational dosimetry was performed to estimate organ absorbed doses resulting from ^{18}F-FDG pediatric use. Two voxelized phantoms, kindly provided by the GSF - Helmholtz Zentrum, were used: "Child" - 7 years child and "Baby" 8-week-old infant. ICRP-128 publication provided the radiopharmaceutical biodistribution of F-18. Tables containing organ absorbed dose and effective dose per unit of injected activity for the two phantoms were obtained. The injected activities were estimated according to data provided in the literature. Images of the absorbed dose distribution were generated from both models. The BEIR VII methodology was used to calculate the risk of cancer induction. The risk of cancer induction (per imaging procedure) for the seven-year-old child was (0.09% ♂ and 0.15% ♀) and for the eight-week old baby was (0.11% ♂ and 0.21% ♀). The ^{18}F-FDG absorbed dose distribution in the children and infants showed some divergences

in comparison to adult data. Probably, the biokinetic data used to children and infants are the main rea-son for this disconnection.
KEYWORDS: ^{18}F-FDG, pediatric use, radiation-induced cancer risk.

DOSIMETRIA COMPUTACIONAL E CÁLCULO DE RISCO DE CÂNCER RADIOINDUZIDO DEVIDO AO USO PEDIÁTRICO DE ^{18}F-FDG

RESUMO: Procedimentos de tomografia por emissão de pósitrons (PET) utilizando ^{18}F-FDG aumentaram significativamente em pacientes pediátricos. O radiofármaco ^{18}F-FDG tem sido frequentemente aplicado em oncologia. A indução do câncer é um dos principais riscos estocásticos da exposição à radiação ionizante do ^{18}F-FDG. A estimativa do risco de câncer induzido por radiação devido a exposições médicas é uma ferramenta importante para a avaliação de risco/benefício. O objetivo deste trabalho foi realizar dosimetria e estimar o risco de indução de câncer devido ao uso pediátrico de ^{18}F-FDG. A dosimetria computacional, usando o código MCNPx, foi realizada para estimar doses absorvidas por órgãos. Foram utilizados dois fantomas voxelizados, gentilmente fornecidos pelo GSF - Helmholtz Zentrum: "Criança" - criança de 7 anos e bebê "bebê" de 8 semanas de idade. Os dados de biodistribuição ^{18}F-FDG foram obtidos na ICRP-128. Foram estimadas doses absorvidas por órgão e dose efetiva por unidade de atividade injetada para os dois fantomas. As atividades injetadas foram estimadas de acordo com os dados fornecidos na literatura. As imagens da distribuição da dose absorvida foram geradas a partir de ambos os modelos. A metodologia da BEIR VII foi utilizada para estimar o risco de indução de câncer. Os resultados obtidos demonstraram que o risco de indução de câncer (por procedimento de imagem com ^{18}F-FDG) para a criança de sete anos de idade foi de (0,09% ♂ e 0,15% ♀) e para o bebê de oito semanas (0,11% ♂ . e 0,21% ♀) .A distribuição de doses absorvidas de ^{18}F-FDG em crianças e bebês mostrou algumas divergências em comparação com os dados de adultos. Provavelmente, os dados biocinéticos utilizados em crianças e bebês são a principal razão para essa desconexão.
PALAVRAS-CHAVE: ^{18}F-FGD, uso pediátrico, risco de câncer radioinduzido.

1 | INTRODUCTION

Nuclear Medicine (NM) has been successfully used in pediatric pathology´s diagnosis and evaluation virtually in all fields of medicine (TREVES; FALONE; FAHEY, 2014). This success occurs largely because NM studies presents the ability to provide patient physiological and metabolic information non-invasively and with low-risk (TREVES; FALONE; FAHEY, 2014).

The positron emission tomography (PET) images using ^{18}F-FDG have increased significantly in pediatric patients (SHAMMAS; LIM; CHARRON, 2009). PET/^{18}F-FDG has often been applied in oncology, usually coupled with anatomical CT images for better localization of the lesion (SHAMMAS; LIM; CHARRON, 2009; STAUSS et al., 2008; THE

ROYAL COLLEGE OF RADIOLOGISTS, 2014). PET/CT scans with ^{18}F-FDG can be used for diagnosis, staging, biopsy planning, radiotherapy planning and evaluation of treatment response. Cardiac and neurological PET/CT studies in children are also reported (THE ROYAL COLLEGE OF RADIOLOGISTS, 2014).

The justification for exposures to ionizing radiation is a general principle of radiation protection (ICRP, 2007). In nuclear medicine, the justification should ensure that medical exposures only occur when the benefits of the medical procedure for the patient outweigh the risks (IAEA, 2015). The benefits and the applicability of the pediatric nuclear medicine are demonstrated in several works (DEPAS et al., 2005; SHAMMAS; LIM; CHARRON, 2009; STAUSS et al., 2008; TATSUMI; MILLER; WAHL, 2007; THE ROYAL COLLEGE OF RADIOLOGISTS, 2014; TREVES; FALONE; FAHEY, 2014; YUAN; ZHANG; LI, 2012). Other researchers bring some concerns about cancer induction/mortality risks from pediatric image protocols and recommendations for dose reduction (ALESSIO et al., 2009; BRENNER et al., 2001). The quantification of the risks and the benefits of radiopharmaceuticals pediatric use is required to better support these practices.An important stochastic risk of ionizing radiation exposure is cancer induction. Several methodologies have been used to estimate the radiation-induced cancer risk(EPA, 2011; ICRP, 2007; NRC, 2006; UNSCEAR, 2015). The aim of this work was to perform dosimetric calculations and estimate radiation-induced cancer risk due to 18F-FDG pediatric use.

2 | MATERIALS AND METHODS

The study was carried out in two steps. Initially the computational dosimetry was performed in two infant voxelized phantoms, simulating ^{18}F-FDG imaging procedures. In the next stage, the radiation-induced cancer risk was estimated considering the absorbed doses calculated for the two models. Absorbed doses from CT procedures, such as anatomical images for localization of lesions or acquisitions for attenuation correction measurements that are usually combined with the ^{18}F-FDG/PET images were not taken into account in this work.

2.1 MCNPx dosimetry

Two voxelized infant phantoms, kindly provided by the GSF -Helmholtz Zentrum, were used for MCNPx simulations (PELOWITZ, 2011). One of the models, called "Child", represents a 7 years child. The other, named "Baby," represents an 8-week-old baby. The phantom masses are 4.2 kg (Baby) and 21.7 kg (Child). The female patient´s images were used in these phantoms construction. The male gonads (testes) were added to the models. Thus, these phantoms can be considered as hermaphrodites. A C++program was developed to adapt the phantoms to MCNPx format. Tissues and organs chemical compositions and densities were obtained at ICRP 110 (ICRP, 2009).The dosimetric

protocols used for MCNPx input-file preparation were described in an earlier publication (MENDES et al., 2017). Some adaptations and specificities concerning to the infant phantoms modified in this work are described hereafter.The F-18 emission probability for the voxels of a given tissue was based on 18F-FDG biodistribution data provided in ICRP 128(ICRP, 2015). Table 1 shows the residence times adopted for the source-organs of "Baby" and "Child" phantoms.The heart wall was not segmented in both models. Thus, the emissions corresponding to this organ were defined in heart's wall and content. In addition, some organs or tissues such as gall bladder wall, lymphatic nodes, ET1 region and breast were not segmented in these models. Thus, for effective dose calculation, some approximations based on absorbed doses of nearby (surrogate) organs were made. ICRP-103 wtand wrweighting factors and calculation methodology were applied (ICRP, 2007)

Source Organs	Residence time - τ (h)	
	"Baby"	"Child"
Urinary Bladder contents	0.16	0.26
Brain	0.21	0.21
Heart Wall	0.11	0.11
Liver	0.13	0.13
Lungs	0.079	0.079
Other organs and tissues	1.7	1.7
Total	2.389	2.489

Table 1: Residence times for "Baby e "Child" source organs according to ICRP 128.

Tables addressing the organ absorbed dose and the effective dose per unit of injected activity for the two phantoms were generated. The calculated values were compared with those provided in ICRP-128 (ICRP, 2015)including biokinetic models, biokinetic data, dose coefficients for organ and tissue absorbed doses, and effective dose for major radiopharmaceuticals based on the radiation protection guidance given in Publication 60(ICRP, 1991. Since this publication had provided data only for 1, 5, 10 and 15 years children, logarithmic interpolation and extrapolation were necessary to find absorbed doses at the 8 weeks and 7 years old child. Images of the absorbed energy distribution were generated from both models.

2.2 Estimation of Radiation-Induced Cancer Risk

The LAR (Lifetime Attributable Risk) of a second cancer incidence induced by an 18F-FDG imaging procedure was estimated according to the methodology of BEIR VII (NRC, 2006). Mean absorbed dose values in organs per unit of injected activity, calculated through "Baby" and "Child" simulations, were used for these estimations. Some guidelines or reference papers have presented the 18F-FDG injected activity per kg of body mass

(ALESSIO et al., 2009; STAUSS et al., 2008; THE ROYAL COLLEGE OF RADIOLOGISTS, 2014; YUAN; ZHANG; LI, 2012). The range of injected activity per body mass in these works was about 3.0 MBq.kg-1to 10.0 MBq.kg-1. Here we have adopted 6.0 MBq.kg-1in order to calculate the total injected activity. Considering the models body weight, the injected activities were defined as 25 MBq to “Baby” and 130 MBq to “Child”.Risk transport for the Brazilian population took into account: i) incidence cancer data, in Brazilian male and female populations, for different cancers by age group, adapted from a study of Instituto Nacional do Câncer –INCA (INCA, 2013); and

ii) the mortality estimates for male and female by age group provided by Instituto Brasileiro de Geografia e Estatística –IBGE(IBGE, 2017).

3 I RESULTS AND DISCUSSION

3.1 MCNPx dosimetry

Table 2 shows organ absorbed dose and effective dose per unit of injected activity calculated for the “Baby” phantom. The organs that presented the highest absorbed doses for this model were heart, urinary bladder wall, lungs, uterus and ovary.

The lowest absorbed doses were observed in the following organs or tissues: skin, small intestine, testicles, stomach wall and endosteum. According ICRP-128 data (ICRP, 2015)including biokinetic models, biokinetic data, dose coefficients for organ and tissue absorbed doses, and effective dose for major radiopharmaceuticals based on the radiation protection guidance given in Publication 60(ICRP, 1991, interpolated to this model at the age of eight weeks, the organs that presented the highest doses were heart, urinary bladder wall, liver, lungs and uterus. The organs that had the lowest absorbed doses according ICRP reference data were skin, breast, brain, red bone marrow and endosteum.

The values of the absorbed dose per organ, calculated in our work for the phantom “Baby” were systematically higher than the reference values of ICRP-128. The only exceptions were data from the heart and the liver. For most organs, deviations were less than ± 30%. The largest differences were found for: lungs (126%), brain (77%), uterus (76%), ovary (62%) and esophagus (51%).

Table 3 shows the absorbed dose per organ and the effective dose per unit of injected activity obtained for the “Child” phantom. The highest absorbed doses per unit of injected activity were found in the following organs: heart, urinary bladder wall, lungs, uterus and liver. The lowest absorbed doses were observed in the skin, breast, muscle, esophagus and endosteum. Among the absorbed doses provided by ICRP-128, interpolated to adjust to the phantom age (seven years), the highest values occurred in the urinary bladder wall, heart, liver, lungs and brain. In addition, in according to this data, the lowest absorbed dose values took place on: skin, breast, red bone marrow, thyroid and endosteum. The

differences between the calculated values for the voxelized models and the interpolated ICRP 128 data were less than ± 15% for most of the organs. The largest deviations were observed for gallbladder wall (61%), urinary bladder wall (-54%), lungs (48%), heart (-32%) and uterus (31%).

Organ	This Work		ICRP 128	Difference[a]
	D/A [mGy/MBq]	SD [mGy/MBq]	D/A [mGy/MBq]	%
Adrenals	1.38E-01	7.76E-04	1.09E-01	26.5%
Endosteum	1.23E-01	8.21E-05	9.83E-02	25.2%
Brain	1.53E-01	1.07E-04	8.66E-02	76.9%
Breast	1.26E-01	4.68E-03	8.66E-02	45.1%
Colon wall (0,57D_ULI + 0,43D_LLI)	1.27E-01	3.18E-04	1.07E-01	18.5%
ET region (thymus/thyroid average)	1.50E-01	4.87E-04	-	-
Gallbladder wall	1.34E-01	1.40E-03	1.07E-01	25.4%
Heart (blood + wall)	5.25E-01	5.77E-04	5.85E-01	-10.2%
Kidneys	1.32E-01	2.99E-04	1.13E-01	17.2%
Liver	1.78E-01	1.60E-04	1.83E-01	-3.0%
Lungs	4.13E-01	5.05E-04	1.83E-01	126.0%
Lymphatic nodes (head&trunk tissues)	1.24E-01	4.54E-05	-	-
Muscles	1.24E-01	4.98E-05	1.03E-01	20.0%
Esophagus	1.52E-01	1.44E-03	1.01E-01	50.8%
Oral Mucosa (head tissue)	1.16E-01	1.05E-04	-	-
Ovary	1.89E-01	2.95E-03	1.17E-01	61.9%
Pancreas	1.38E-01	9.23E-04	1.17E-01	17.9%
RBM	1.27E-01	9.01E-05	9.00E-02	41.1%
Salivary Glands (head tissue)	1.16E-01	1.05E-04	-	-
Small intestine	1.21E-01	2.55E-04	1.13E-01	7.4%
Stomach wall	1.23E-01	5.65E-04	1.03E-01	19.1%
Skin	9.78E-02	7.95E-05	7.76E-02	26.0%
Spleen	1.30E-01	4.15E-04	1.02E-01	27.6%
Thymus	1.52E-01	5.15E-04	1.01E-01	50.3%
Thyroid	1.33E-01	1.47E-03	1.01E-01	32.4%
Urinary bladder wall	5.04E-01	1.77E-03	4.45E-01	13.2%
Uterus/cervix	2.44E-01	1.80E-03	1.38E-01	76.2%
Prostate [b]	2.44E-01	1.80E-03	-	-
Testes	1.23E-01	1.34E-03	1.02E-01	19.8%
Effective Dose (mSv/MBq)	1.87E-01	1.20E-03	1.45E-01	28.6%

Table 2 - 8w infant organ absorbed dose and effective dose per unit of ^{18}F-FDG injected activity (D/A) calculated in this work compared with the ICRP interpolated value.

a - Difference = ((This work value - ICRP value)/ICRP value)*100

b - Considered the same as uterus absorbed dose for effective dose calculation

Organ	This Work		ICRP 128	Difference[a]
	D/A [mGy/MBq]	SD [mGy/MBq]	D/A [mGy/MBq]	%
Adrenals	3.49E-02	3.84E-04	3.15E-02	10.7%
Endosteum	2.73E-02	1.33E-05	2.82E-02	-3.2%
Brain	3.89E-02	3.11E-05	4.42E-02	-12.0%
Breast (trunk skin)	2.37E-02	3.08E-05	2.38E-02	-0.6%
Colon wall (0,57D_ULI + 0,43D_LLI)	3.23E-02	8.46E-05	3.17E-02	1.8%
ET region (mucous membrane)	3.06E-02	1.25E-04	-	-
Gallbladder wall (liver)	5.01E-02	4.51E-05	3.11E-02	60.8%
Heart (blood + wall)	1.15E-01	1.27E-04	1.70E-01	-32.1%
Kidneys	3.17E-02	6.00E-05	3.23E-02	-1.9%
Liver	5.01E-02	4.51E-05	5.33E-02	-6.0%
Lungs	7.84E-02	9.40E-05	5.29E-02	48.3%
Lymphatic nodes (head&trunk tissues)	2.98E-02	8.57E-06	-	-
Muscles (soft tissue)	2.68E-02	6.69E-06	2.96E-02	-9.2%
Esophagus (mucous membrane)	2.73E-02	1.53E-04	2.92E-02	-6.6%
Oral Mucosa (mucous membrane)	2.73E-02	1.53E-04	-	-
Ovary	3.68E-02	4.75E-04	3.47E-02	6.2%
Pancreas	3.35E-02	1.44E-04	3.32E-02	0.9%
RBM	2.94E-02	1.55E-05	2.67E-02	10.3%
Salivary Glands (head tissue)	2.60E-02	2.60E-05	-	-
Small intestine (wall + contents)	3.31E-02	3.97E-05	3.23E-02	2.5%
Stomach wall	2.88E-02	9.80E-05	2.89E-02	-0.4%
Skin	2.11E-02	1.80E-05	2.10E-02	0.5%
Spleen	3.01E-02	6.63E-05	2.86E-02	5.5%
Thymus	3.50E-02	1.51E-04	2.92E-02	20.0%
Thyroid	2.86E-02	3.24E-04	2.78E-02	3.1%
Urinary bladder wall	8.00E-02	2.32E-04	1.74E-01	-54.1%
Uterus/cervix	5.64E-02	2.59E-04	4.29E-02	31.4%
Prostate [b]	5.64E-02	2.59E-04	-	-
Testes	2.86E-02	5.07E-04	2.96E-02	-3.1%
Effective Dose (mSv/MBq)	3.92E-02	1.13E-04	4.50E-02	-12.8%

Table 3 - 7y children organ absorbed dose and effective dose per unit of ^{18}F-FDG injected activity (D/A) calculated in this work compared with ICRP interpolated value.

[a] - Difference = ((This work value - ICRP value)/ICRP value)*100

[b] - Considered the same as uterus absorbed dose for effective dose calculation

Considering the phantom masses (4.2 kg - “Baby” and 21.7 kg “Child”) and the injected activity per unit of mass (6.0 MBq/kg) the effective dose for the Baby model was 4.7 mSv and for the Child model, the value was 5.1 mSv.

Tridimensional images absorbed energy distribution were generated for both models. Figure 1 show coronal slices of “Baby”, “Child” models showing the energy deposition pattern due to ^{18}F-FDG injection using ICRP 128 residence times (ICRP, 2015)including biokinetic models, biokinetic data, dose coefficients for organ and tissue absorbed doses,

and effective dose for major radiopharmaceuticals based on the radiation protection guidance given in Publication 60(ICRP, 1991. A coronal image of RCP_AM voxelized model showing absorbed energy distribution due to ^{18}F-FDG injection was also added to Figure 1 for comparison.

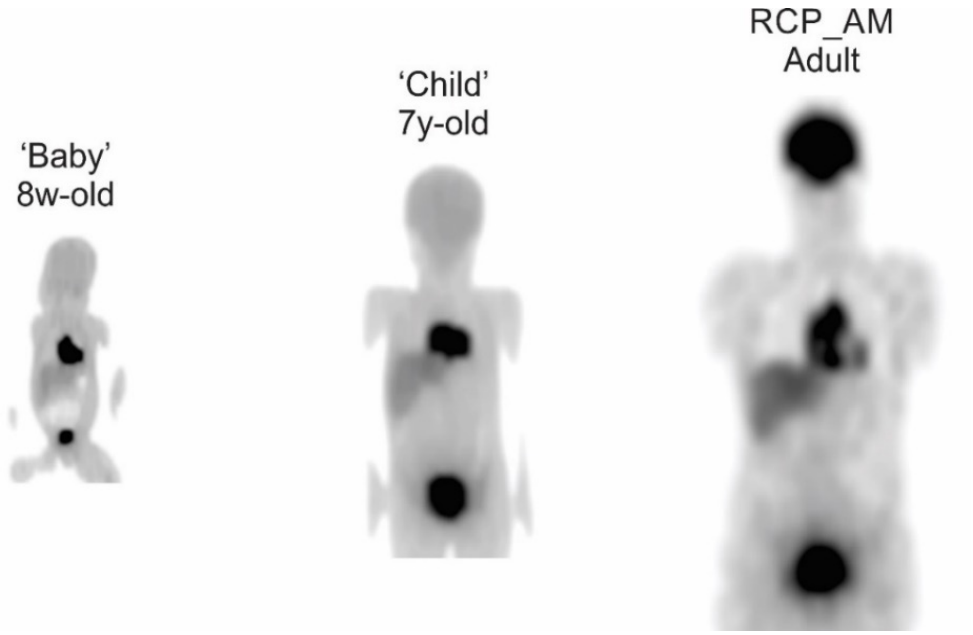

Figure 1 - Coronal slices of "Baby", "Child" and RCP_AM voxelized models showing the energy deposition pattern due to ^{18}F-FDG injection using ICRP 128 residence times.

3.2 Estimation of Radiation-Induced Cancer Risk

Tables 4 and 5 present the lifetime attributable risk (LAR) of incidence of ^{18}F-FDG induced cancer in male and female children. The organs absorbed dose values previously calculated for the "Child" and "Baby" phantoms were used to estimate the risk, as well as the injected activities defined in this work (25 MBq - Baby; 130 MBq - Child).

Lung tumors presented the highest occurrence probability for both sexes and ages. Among the girls, breast cancer has also showed a high incidence. The probability of occurrence of a radiation-induced cancer was higher among the girls than among the boys to the two ages studied. The total risk of cancer induction, per imaging procedure, for the seven-year-old child was (0.09% ♂ and 0.15%♀) and for the eight-week old baby was (0.11% ♂ and 0.21%♀).

Organ	Male "Baby" – 8w old		Male "Child" – 7y old	
	D [mGy]	LAR [Cases/100.000 Exposed persons]	D [mGy]	LAR [Cases/100.000 Exposed persons]
Stomach	3.1	5	3.8	5
Colon	3.2	6	4.2	7
Liver	4.5	3	6.5	3
Lungs	10.4	26	10.2	20

Prostate	6.1	5	7.3	5
Urinary bladder	12.7	16	10.4	11
Other Solid Cancer	3.2	41	4.2	27
Thyroid	3.4	4	3.7	2
All Solid Cancers	-	105	-	79
Leukemia	3.2	6	3.8	5
All Cancers	-	111	-	85

Table 4 - Lifetime attributable risk of cancer incidence calculated for 8 weeks old and 7 years old male infants of the Brazilian population, considering a ^{18}F-FDG injected activity of 25 MBq for “Baby” and 130 MBq for “Child”.

Organ	Female “Baby” – 8w old		Female “Child” – 7y old	
	D [mGy]	LAR [Cases/100.000 Exposed persons]	D [mGy]	LAR [Cases/100.000 Exposed persons]
Stomach	3.1	6	3.8	6
Colon	3.2	4	4.2	5
Liver	4.5	2	6.5	2
Lungs	10.4	55	10.2	42
Breast	3.2	38	3.1	27
Uterus/cervix	6.1	5	7.3	4
Ovary	4.8	4	4.8	3
Urinary bladder	12.7	18	10.4	12
Other Solid Cancers	3.2	46	4.2	30
Thyroid	3.4	29	3.7	18
All Solid Cancers	-	205	-	148
Leukemia	3.2	5	3.8	4
All Cancers	-	210	-	152

Table 5 - Lifetime attributable risk of cancer incidence calculated for 8 week old and 7 years old female infants of the Brazilian population, considering a ^{18}F-FDG injected activity of 25 MBq for “Baby” and 130 MBq for “Child”.

4 I DISCUSSION

The absorbed dose values calculated for the phantom "Baby" were systematically higher than the reference values of ICRP-128 (ICRP, 2015), observed in table 2. The extrapolation of the ICRP values was performed taking as base the age of the phantom. The weight-versus-age tablesindicate that for an eight week old baby the expected weight (-1SD / Median / + 1SD) is ♀) 4.4 / 5.0 / 5.7 kg and ♂) 4.8 / 5.4 / 6.1 kg(WHO, 2008). Even for a female baby the phantom mass (4.2 kg)is relatively low for this age. This factor may be the main reason for the overestimations observed in the calculated values, since usually it can be stated that the lower the mass of the model, the higher the dose per unit of injected activity (ALESSIO et al., 2009). Weight extrapolation (and not by age) would be more appropriate in this case. In addition, logarithm extrapolation could be inadequate for reference data.

A good agreement was found between the data calculated for the “Child” model and

the ICRP-128 reference values (ICRP, 2015)interpolated for the age of 7 years, presented in table 3. The total mass of this model (21.7 kg) is slightly below average, but within the expected range for that age. The World Health Organization(WHO, 2008)establishes the weight of (♀) 20.1 / 23.4 / 27.6 kg and (♂) 20.9 / 23.9 / 27.7 kg (-1SD / Median / + 1SD) for 7 years and 6 months old children.

Some organs in both models ("Baby" and "Child") show large differences between calculated values and reference values based on ICRP-128 data (ICRP, 2015). Such fact has already been reported in other studies comparing simulation results using voxelized models with those usingstylized models (HADID; GARDUMI; DESBREÉ, 2013; ZANKL et al., 2012). Usually these disparities are related to the diversity of: i) anatomy of the models (shape and position of the organs); ii) chemical composition and density of the tissues; iii) differences in the methodology of the energy transport of particles (photons, electrons and positrons). It is possible, for some organs, to identify the main cause of divergences. The voxelized models has often underestimated the absorbed dose on the wall of the urinary bladder when compared with analytical models (HADID; GARDUMI; DESBREÉ, 2013; ZANKL et al., 2012). In fact, all organs holding a wall narrower than the voxel dimensions may present this type of problem. A partial volume effect can occur, as the voxelized models cannot represent an organ wall as thin as the real one. Analytical models do not have such a limitation. In the case of the heart, the voxelized "Baby" and "Child" models do not have distinguished between heart wall and content (blood). Thus, the emissions in this organ were distributed in these two compartments. The ICRP stylized models have this distinction. Thus, all the emissions related to heart residence-time occur only in the wall of the organ. In addition, the absorbed dose wasmeasured only in the cardiac wall.

The analysis of the absorbed dose values per organ for 18F-FDG pediatric patients show some intriguing data. For example, the absorbed dose in the brain was lower than the liver absorbed dose in all the studied cases, including ICRP reference values (ICRP, 2015). Indeed, according to ICRP-128 data, brain absorbed dose for a one-year-old child is only greater than the absorbed dose in four organs/tissues: muscles, red marrow, breast and skin. Brain fractional activity is higher than liver’s, for adults (HAYS et al., 2002; ICRP, 2015), as can be seen in Figure 2.

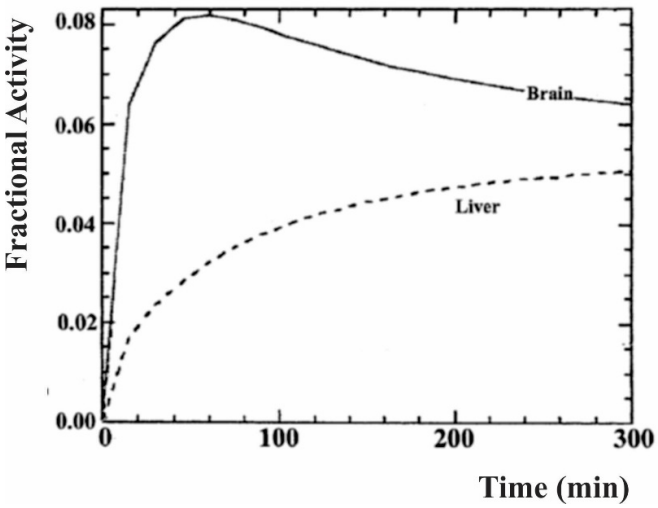

Figure 2 - Decay corrected time-activity curves for brain and liver after ^{18}F-FDG intravenous injection in adults – adapted from work of Hays et al., 2002 [26].

As the liver has a volume slightly larger than brain volume, the activity concentration must higher on the brain. In adults, the brain has the third largest absorbed dose, only smaller than the urinary bladder wall and heart wall (ICRP, 2015)including biokinetic models, biokinetic data, dose coefficients for organ and tissue absorbed doses, and effective dose for major radiopharmaceuticals based on the radiation protection guidance given in Publication 60(ICRP, 1991. Based on the assumption that the infant brain should have a higher uptake per unit mass than the liver, as observed for adults, brain low absorbed doses would not be expected for infants.

This brain uptake inconsistency can also be observed in “Child” and “Baby” images in Figure 1. The images of the infant models do not match ^{18}F-FDG literature images (Figure 3) (ALESSIO et al., 2009; FREEBODY; WEGNER; ROSSLEIGH, 2014)the dose from PET/CT protocols that use a fixed CT technique of 120 mAs and 120 kVp. The approximate, conservative estimate of additional lifetime attributable risk (LAR. On the other hand, ^{18}F-FDG image of RCP_AM has good agreement with images found in literature (OTSUKA et al., 2007). ^{18}F-FDG images show that the brain has a higher uptake than the liver, no matter the patient age (ALESSIO et al., 2009; FREEBODY; WEGNER; ROSSLEIGH, 2014; OTSUKA et al., 2007).

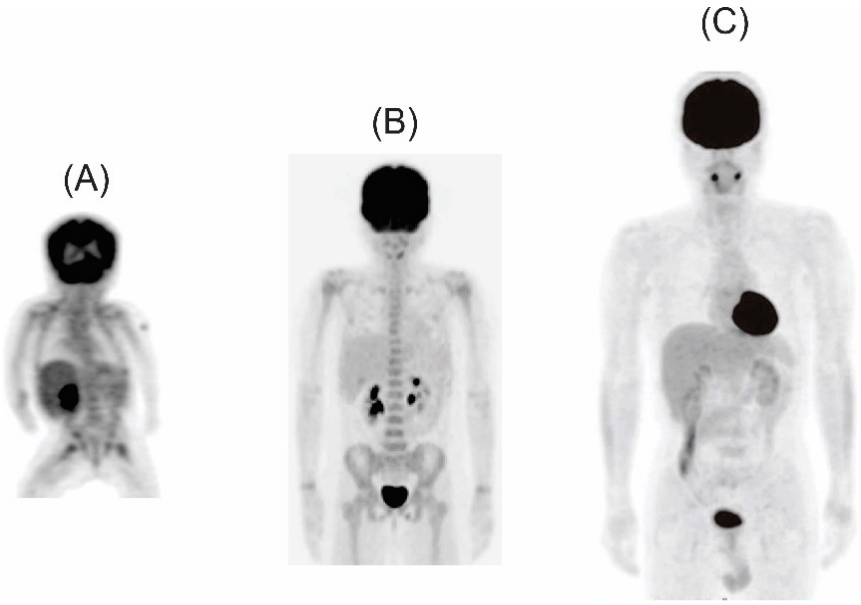

Figure 3 - Coronal slices of ^{18}F-FDG uptake found in literature for individuals with different ages: (A) - 16 week old and 6 kg baby, adapted from Alessio et al., 2009. (B) – 8 years old female, adapted from Freebody et al., 2014. (C) – 45 years old male, adapted from Otsuka et al., 2007.

The ICRP-128 biodistribution data for 18F-FDG should be obtained from adult subjects images/experiments. According to ICRP-128 (ICRP, 2015), the adaptation of these data for child's models consists only in the reduction of the urinary bladder content residence-times for five-years and one-year old children. The proportion between specific organ masses and the whole body mass changes considerably with age. The brain, for example, accounts for about 11% of the whole body mass in newborns. In adults, brain mass is only about 2% of whole body weight. The same occurs, in a smaller proportion, for the other source organs: urinary bladder (1.1% / 0.3%), heart (1.3% / 0.5%) and liver (3.7% / 2.5%) -(newborn / adult). The lung is the only exception. In the newborn, it represents 1.7% of the whole body mass and in the adult, 1.6% (ICRP, 2002). Therefore, using the same residence time for adult and newborn organs can generate distortions, such as that reported in the brain. In fact, the application of this methodology to 18F-FDG should result in lower absorbed doses for urinary bladder, heart, liver and especially the brain. On the other hand, overestimations are expected to the other organs of the infants.

The cancer induction risk due to pediatric 18F-FDG/PET was higher for female younger children. The absorbed doses in "Baby" and "Child" radiosensitive organs were quite similar, as shown in Tables 4 and 5. The higher absorbed dose values per injected-activity of the "Baby" phantom were compensated by the lower injected activity. The effective dose for these two models was also similar (Baby: 4.7 mSv; Child: 5.1 mSv). These results are in accordance with Alessio et al., (2009) work. They found an 18F-FDG effective dose of 5.0 mSv for infants with 6.0 to 7.4 kg weight range and 5.3 mSv for 18.5 to 22.4 kg. Nevertheless, the risk of cancer incidence was 30 to 40% higher for the "Baby" model. The risk of cancer induction increases considerably as the age of the patient decreases. This explains the higher values for the younger model. Lung cancer

(and breast cancer, in the case of female children) had the highest contribution to the total number of cases of radiation-induced cancer. This is a matter of concern since lung cancer can often be associated with low survival rates (~18%) (SIEGEL; MILLER; JEMAL, 2017). The incidence risk values for “all cancers” obtained in this work were 0.21% (♀)/0.11% (♂) for "Baby" and 0.15% (♀)/0.09% (♂) for "Child". Radiation-induced cancer risk from pediatric 18F-FDGimaging is not negligible; especially if we consider that,the risk calculated excludes the CT absorbed dose component. In addition, more than one 18F-FDG imaging study is often required,as for the treatment response evaluation. The Alessio et al., 2009 study found values slightly larger: 0.34% (♀)/0.18% (♂) for the newborn (6.0 to 7.4 kg) and 0.28% (♀)/0.15% (♂) for a Child (18.5 to 22.4 kg), but they consider PET and CT absorbed doses in the estimations(ALESSIO et al., 2009).

5 I CONCLUSION

MCNPx computational dosimetry for pediatric ^{18}F-FDG PET was performed for the “Baby” and “Child” phantoms and the radiation-induced cancer risk was estimated based on the absorbed dose values obtained for the radiosensitive organs. Lung cancer incidence represented the greatest contribution to the total estimated cases.

The whole risk of cancer induction due to pediatric ^{18}F-FDF PET, for the Brazilian population, was 0.21% (♀) to 0.11% (♂) for an 8-week-old baby and 0.15% (♀) a 0.09% (♂) for a seven-year-old child. This value may be considered high since the CT component of the absorbed dose has not been evaluated in this study and more than one imaging procedure may be required, depending on the reason for which the image was taken (detection, staging, therapeutic monitoring, etc.). The quantification of the benefits of pediatric ^{18}F-FDG PET also should be carried out in future studies, allowing better evaluation of the risk/benefit ratio for applying this technique.

In addition, the use of the same residence times obtained for adults for ^{18}F-FDG infantile dosimetry generates distortions in the calculated absorbed dose values. Residence times obtained from children’s images would be the ideal option. More accurate residence time data will become available with the increasing of pediatric ^{18}F-FDG. At this time, methodologies for adapting adult data to children should be developed and applied.

A future study will present a methodology suggested by our group for the adaptation of adult biokinetic data to children.

6 I ACKNOWLEDGMENTS

We would like to thank the Laboratório de Metrologia de Nêutrons of the Instituto de Radioproteção e Dosimetria (IRD/CNEN) for allowing the access and use of the cluster

Orion to perform the simulations in MCNPx. The following Brazilian institutions supported this research project: Fundação de Amparo à Pesquisa de Minas Gerais (FAPEMIG), and Conselho Nacional de Desenvolvimento Científico e Tecnológico (CNPq) projeto REBRAT-SUS, 2013-2017.

REFERENCES

ALESSIO, A. M. et al. Weight-based, low-dose pediatric whole-body PET/CT protocols. **Journal of Nuclear Medicine**, v. 50, n. 10, p. 1570–1578, 2009.

BRENNER, D. J. et al. Estimated Risks of Radiation-Induced Fatal Cancer from Pediatric CT. **American Roentgen Ray Society**, v. 176, n. February, p. 289–296, 2001.

DEPAS, G. et al. 18F-FDG PET in children with lymphomas. **European Journal of Nuclear Medicine and Molecular Imaging**, v. 32, n. 1, p. 31–38, 2005.

EPA. **EPA Radiogenic Cancer Risk Models and Projections for the U . S . Population**. Washington, DC. EUA: U.S. Environmental Protection Agency., 2011.

FREEBODY, J.; WEGNER, E. A.; ROSSLEIGH, M. A. 2-deoxy-2-(18 F)fluoro-D-glucose positron emission tomography/computed tomography imaging in paediatric oncology. **World Journal of Radiology**, v. 6, n. 10, p. 741, 2014.

HADID, L.; GARDUMI, A.; DESBREÉ, A. **Evaluation of absorbed and effective doses to patients from radiopharmaceuticals using the ICRP 110 reference computational phantoms and ICRP 103 formulation**. **Radiation Protection Dosimetry**. [S.l: s.n.]. , 2013

HAYS, M. T. et al. MIRD dose estimate report no. 19: Radiation absorbed dose estimates from 18F-FDG. **Journal of Nuclear Medicine**, v. 43, n. 2, p. 210–214, 2002.

IAEA. Radiation Protection in Medicine: Setting the Scene for the Next Decade. **Proceedings of an International Conference**, n. December, p. 2–17, 2015. Disponível em: <https://www.iaea.org/publications/10611/radiation-protection-in-medicine-setting-the-scene-for-the-next-decade>.

IBGE. Tábua Completa de Mortalidade para o Brasil - 2015. **Instituto Brasileiro de Geografia e Estatística. Ministério da Saúde.**, p. 15, 2017. Disponível em: <ftp://ftp.ibge.gov.br/Tabuas_Completas_de_Mortalidade/Tabuas_Completas_de_Mortalidade_2016/tabua_de_mortalidade_2016_analise.pdf>.

ICRP. Adult Reference Computational Phantoms. ICRP Publication 110. **Annals of the ICRP**, v. 39, n. 2, p. 21–45, 2009.

ICRP. Basic anatomical and physiological data for use in radiological protection: reference values. **Annals of the ICRP**, v. 32, n. 3–4, p. 1–277, 2002.

ICRP. Radiation Dose to Patients from Radiopharmaceuticals: a Compendium of Current Information Related to Frequently Used Substances. **Annals of the ICRP**, v. 44, n. 2 Suppl, p. 7–321, 2015.

ICRP. The 2007 Recommendations of the International Commission on Radiological Protection. **Icrp 103**, p. 2007–2007, 2007.

INCA. **Cancer in Brazil - Data from the Population-Based Registries**. [S.l.]: National Cancer Institute José Alencar Gomes da Silva, 2013. v. IV.

MENDES, B. M. et al. OF Desenvolvimento de protocolos de dosimetria interna empregando o código MCNPx e fantomas voxelizados de referência da ICRP 110. v. 01, p. 1–14, 2017.

NRC. **Health risks from exposure to low levels of ionizing radiation: BEIR VII Phase 2**. Washington, D.C., EUA: [s.n.], 2006.

OTSUKA, H. et al. FDG-PET/CT for cancer management. **Journal of Medical Investigation**, v. 54, n. 3–4, p. 195–199, 2007.

PELOWITZ, D. B. **Mcnpx User's Manual - Version 2.7.0**. . [S.l: s.n.], 2011.

SHAMMAS, A.; LIM, R.; CHARRON, M. Pediatric FDG PET / CT : Physiologic Uptake , Normal Variants , and Benign Conditions. **RadioGraphics**, v. 29, n. 5, p. 1467–1486, 2009.

SIEGEL, R. L.; MILLER, K. D.; JEMAL, A. Cancer statistics, 2017. **CA: A Cancer Journal for Clinicians**, v. 67, n. 1, p. 7–30, 2017.

STAUSS, J. et al. Guidelines for 18F-FDG PET and PET-CT imaging in paediatric oncology. **European Journal of Nuclear Medicine and Molecular Imaging**, v. 35, n. 8, p. 1581–1588, 2008.

TATSUMI, M.; MILLER, J. H.; WAHL, R. L. 18F-FDG PET/CT in evaluating non-CNS pediatric malignancies. **Journal of Nuclear Medicine**, v. 48, n. 12, p. 1923–1931, 2007.

THE ROYAL COLLEGE OF RADIOLOGISTS. Guidelines for the use of PET-CT in children, Second edition. 2014. Disponível em: <www.rcr.ac.uk>.

TREVES, S. T.; FALONE, A. E.; FAHEY, F. H. Pediatric nuclear medicine and radiation dose. **Seminars in Nuclear Medicine**, v. 44, n. 3, p. 202–209, 2014. Disponível em: <http://dx.doi.org/10.1053/j.semnuclmed.2014.03.009>.

UNSCEAR. **UNSCEAR 2012 Report to the General Assembly**. New York, USA: United Nations Scientific Committee on the Effects of Atomic Radiation, 2015.

WHO. **The who child growth standards**. Disponível em: <https://www.who.int/childgrowth/standards/en/>.

YUAN, L.; ZHANG, N.; LI, C. PET / CT application in pediatric oncology. p. 1–8, 2012.

ZANKL, M. et al. Electron specific absorbed fractions for the adult male and female ICRP/ICRU reference computational phantoms. **Physics in Medicine and Biology**, v. 57, n. 14, p. 4501–4526, 2012.